Effect of warm shot peening treatments on surface properties and corrosion behavior of AZ31 magnesium alloy

L.B. Peral[a*], A. Zafra[a], S. Bagherifard[b], M. Guagliano[b], I. Fernández-Pariente[a]

a Department of Material Science and Metallurgical Engineering, University of Oviedo, Gijón, Spain
b Department of Mechanical Engineering, Politecnico di Milano, Milan, Italy

*Corresponding author: luisborjapm@gmail.com (L.B.Peral)

Abstract
Magnesium alloys are considered as a suitable choice for temporary biodegradable implants due to their biocompatible and biodegradable properties, able to avoid a second surgery when implant removal is needed. Nevertheless, nowadays one of the shortcomings of magnesium-based materials is their poor corrosion resistance and the associated high corrosion rate. This fact considerably hinders their application in biomedical field. The aim of this work is to induce a severe plastic deformation on the upper layer of the AZ31 Mg alloy in order to modulate its surface properties to slow down the kinetics of the corrosion damage. Specimens were submitted to conventional and severe shot peening treatments at room temperature, 240°C (near recrystallization temperature) and 360ºC (above recrystallization temperature); the specimens were then analyzed in terms of grain refinement, surface roughness, work hardening, and residual stresses. Potentiodynamic polarization tests were also performed to evaluate the influence of the shot peening treatments on the specimens' corrosion resistance. The results evidenced surface roughness as the most influential factor in corrosion behavior, although for the specimens with similar roughness, also the effect of grain size is notable.

Key words: warm shot peening, microstructure, grain size, corrosion behavior.

1 Introduction

Magnesium alloys have attracted considerable interest in a wide range of applications due to their low density, high specific strength, and stiffness [1]. The low formability and poor mechanical properties of pure magnesium at room temperature have brought more attention to various magnesium alloys that can present a combination of improved mechanical properties and corrosion resistance [2-3]. Aluminum (Al), Calcium (Ca), Zinc (Zn), Zirconium (Zr), Strontium (Sr), and rare earth elements (REEs) such as Yttrium (Y), Gadolinium (Gd), Lanthanum (La), and Dysprosium (Dy), are the most commonly used alloying elements, with high potential in improving the performance of magnesium-based materials [3].

During the last decades many researchers have focused on taking benefit from the superior characteristics of magnesium-based materials to be used for biomedical implants, replacing stainless steel or titanium alloys that are currently used for bone tissue applications [4, 5]. Magnesium stiffness is much closer to that of the natural bone compared to the currently used metallic biomaterials and thus it would reduce the stress shielding effect, which is a notable advantage from the point of view of bone-metal interface stability [6, 7]. In addition to being bio-compatible, magnesium is also biodegradable, and its degradation products, not only are non-toxic, but also have been reported to exhibit positive effects on bone growth: the release of Mg^{2+} into the fracture site is reported to help bone fracture healing, due to the capacity of magnesium to promote CGRP-mediated osteogenic differentiation [8]. Magnesium is already present in the body as an essential element for many biochemical functions, and its excess can be easily eliminated by the urine [9]. Due to their biodegradable and biocompatible properties, magnesium alloys have been considered as a suitable choice for temporary biodegradable implants such as cardiovascular stents [10] and fixation plates, avoiding the need to a second removal surgery [11]. Nevertheless, the poor corrosion resistance of the magnesium-based materials in physiological environment that has considerably hindered the expansion of their

application in biomedical field [3]. The significantly high and uncontrolled corrosion rate will cause unexpected and fast degradation of the magnesium implant, leading to fast degradation before the healing of the broken bone tissue [12]. In addition, magnesium's fast degradation can create local gas cavity, which can be damaging for bone healing and cause pain for the patient [13-15]. In the case of stents, it is expected that bubble generation would lead to embolism; this could induce serious risk for the survival of the patient.

Therefore, although magnesium alloys present interesting characteristics for orthopedic applications because of their high specific ratio, biodegradability and biocompatibility, their rapid degradation are nowadays a notable limit on their wider application. Multiple approaches, including chemical [16-19] and mechanical [20, 21] surface treatments, have been suggested to address the fast degradation issue of magnesium-based materials. A general idea, which has attracted the researcher's attention, is to focus on controlling the surface layer properties, since corrosion, stress corrosion cracking and other damage mechanisms can be highly controlled by modulating the surface characteristics of the material. Chemical approaches focus on alloying techniques that minimize corrosion between different phases; also, creating protective coating layers have been suggested and investigated in an attempt to control and delay the degradation rate [3].

Besides, different studies have also demonstrated that microstructural characteristics particularly grain dimension, can influence corrosion resistance. Although there are some contrasting results in this case [22], many studies have shown that smaller grain dimensions can lead to higher resistance to corrosion because of the higher amount of grain boundaries that act as corrosion barriers [23-24]. Kovaci et al. studied the effect of severe plastic deformation induced by different shot peening treatments on the corrosion behavior of an AISI 4140 low-alloy steel [25]. Electrochemical analyses methods indicated that the corrosion resistance of the material increased with the increasing shot peening intensity due to grain refinement and formation of sub-grains. On the other hand, corrosion resistance of the WE43 Magnesium alloy was analyzed in 0.9% NaCl solution after applying different shot peening treatments [26]. Corrosion current density of the shot-peened samples were reduced by 16%−32%, contributing to increase the corrosion resistance of the material. This was because the residual compressive stresses induced on the metal surface by shot peening treatments, contributed to increase the passivation film ($MgOH_2$) density, which could protect magnesium alloys substrate against being destructed.

The effect of shot peening on corrosion behavior of 316L stainless steel was investigated by Azar et al. in Ringer's solution [27]. They indicated that increasing the shot peening time promotes the break-down potential of the passive layer to increase and corrosion current density and corrosion rate in the passive region to decrease (in comparison to non-treated samples), what contributed to improve pitting corrosion resistance.

Severe plastic deformation methods are well known to be able to induce grain refinement in metallic materials. Among these processes, shot peening (SP) applied with high energy parameters (also known as severe shot peening (SSP)) has been recognized to be able to obtain notable grain refinement down to ultrafine and nano regime on the surface top layer of the treated metals. SP consists of impacting a flux of spherical shots against the metallic surface, inducing compressive residual stress field and work hardening of the upper layer of the material, while increasing surface roughness [28-31]. In SSP treatment the kinetic energy of the process is enhanced, by increasing the Almen intensity of the shot stream and the exposure time of the components to the shot flux; these parameters promote the favorable condition for grain size refinement on the top surface layer of material [32-34].

With the aim of modifying surface properties in magnesium alloys, several researchers have applied standard shot peening treatments to various magnesium alloys with controlled parameters. In all cases positive effects regarding improved mechanical properties have been reported [35-37]. However, based on the reported data, the choice of process parameters in terms of shot size, shot material, velocity and surface coverage are of great importance in case of magnesium alloys, as these materials have shown a significant sensitivity exhibited in the form of a saturation limit over which higher process parameters would result in reduced mechanical performance [38]. Previous studies have disclosed a limited depth and extent of residual stresses as well as the thickness of the layer of material that can be affected by standard shot peening at room

temperature, using the optimized treatment parameters [35, 39]. Regarding the application of SSP, a recent study performed by some of the authors showed notable grain refinement on the surface of AZ31 alloy specimens [35]. Also in this case, the thickness of the affected layer was reported to be less than expected. Indeed, the hexagonal close-packed network (HCP) microstructure of magnesium-based materials is recognized to impede the possibility to activate most of slipping planes except the ones of basal planes, at room temperature. Consequently, twinning becomes the more prevalent and favorable deformation mechanism; this explains the poor formability and plastic deformation of magnesium at room temperature. It is expected that higher temperatures will tackle this problem by allowing prismatic and pyramidal planes to slip, as higher temperature is supposed to reduce their critical resolved shear stress (CRSS) [40]. In this regard, Huang et al. [39], reported that at higher temperatures, Mg–9Gd–2Y alloy specimens can be more plastically deformed and even less damaged by shot peening; this higher tendency to deform, can also offer the chance to use higher Almen intensity on magnesium alloys, and extend the threshold saturation limit where the sudden drop in fatigue strength improvement is reported to occur for shot peened magnesium-based materials.

According to the above mentioned issues, in this work AZ31 magnesium alloy, considered of interest in aircraft, automotive [41] and biomedical [3] industry was subjected to shot peening treatments using different kinetic energies that can be categorized as conventional and severe treatments both at room temperature, at 240˚C (near recrystallization temperature) and at 360˚C (over recrystallization temperature). The treated specimens were critically analyzed with the aim to assess the changes introduced in their surface layer in terms of roughness, grain structure, work hardening, residual stresses, and thickness of the affected zone, depending on the treatment conditions. Corrosion behavior was also studied by means of potentiodynamic polarization curves and the obtained data were discussed in relation with the changes introduced in the material.

2 Experimental procedure

2.1 Material and specimens

Specimens of AZ31 magnesium alloy were cut from a cold rolled sheet of 6 mm in thickness (Alfa Aesar GmbH, GE), with parallelepiped geometry of 20×20×6 mm^3. The nominal chemical composition of the alloy is presented in Table 1.

Table 1. Chemical composition of AZ31 (% in weight)

Mg	Al	Zn	Mn	Si	Cu	Ca	Fe	Ni
97	2.5-3.5	0.7-1.3	0.2	0.05	0.05	0.04	0.005	0.005

Initially all the specimens were annealed at 400ºC for 10 h in order to attain microstructural homogenization. Then, the specimens were submitted to traditional SP and SSP treatments under different temperatures of room temperature (RT), 240ºC and 360ºC.

2.2 Warm shot peening treatments

The specimens were submitted to different shot peening treatments with varied amounts of kinetic energy (conventional and severe treatments). Taking into account the deformation limit of the material (HCP crystalline network [39, 40]), the shot peening treatments were performed at various temperatures to assess the possibility of increasing the thickness of the affected layer, by increasing the thermal energy. The considered treatment temperatures include 240°C, corresponding to the recrystallization temperature, [39] and 360°C, above the recrystallization temperature. Room Temperature treatment (RT) was also performed to serve as a reference.

Specimens were heated by means of Joule effect and the temperature was continuously controlled during the treatment by a thermocouple that was connected to a temperature control device. To maintain the temperature constant at the chosen value, current steps were controlled using a regulator device. Figure 1 shows an image of the home-built specimen heating device.

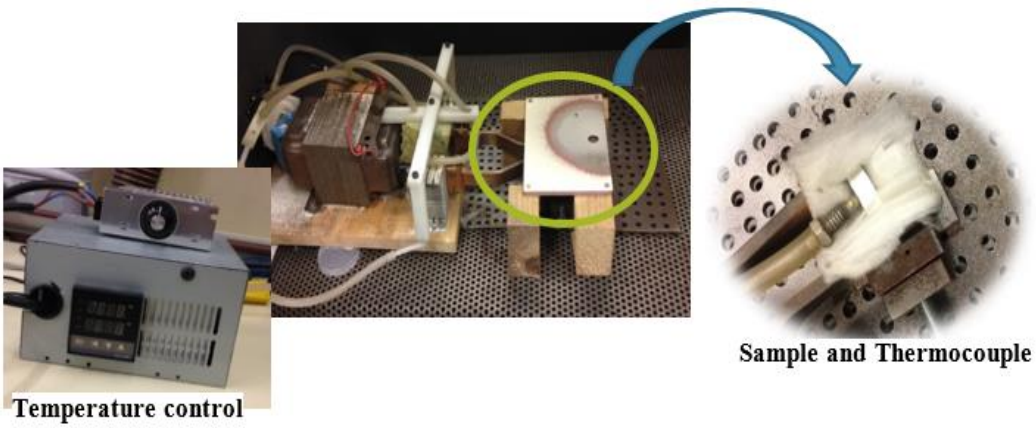

Figure 1. Home-built system developed to perform warm SP treatments

The specimens were shot peened in an air blast SP machine, using Zirshot Y 300 shots, under an Almen Intensity of 10A and three different levels of coverage: 100% (2s) (conventional), 500% (7s) and 1000% (14s); the last two sets of parameters correspond to severe treatments. All these parameters are of great importance in the SP process, as they are directly related to the total kinetic energy transmitted to the material and thus, will have an important influence on the induced plastic strain. SP parameters are listed in Table 2. Chemical composition, average diameter, density and hardness of Zirshot Y300 shots are also shown in Table 3.

Table 2. Shot peening process parameters

Treatment	Shot	Almen Intensity	Coverage	Time (s)	Temperature (ºC)
Conventional	Zirshot Y 300	10A	100%	2s	RT; 240; 360
Severe 500	Zirshot Y 300	10A	500%	7s	RT; 240; 360
Severe 1000	Zirshot Y 300	10A	1000%	14s	RT; 240; 360

Table 3. Chemical composition (wt.%) and mechanical properties of shots

	Chemical composition (%wt)	Diameter (mm)	Density (g/cm^3)	Hardness (HV)
Zirshot Y300	ZrO_2 >75% - SiO_2<25%	~0.3	4.6	1000

2.3 Microstructural characterization

Microstructural changes induced by the SP treatments on the AZ31 specimens were observed using an optical microscope (Nikon Epiphot 300). The SP treated specimens were cut through their cross section with the aim to analyze the microstructure from the surface to the inner core of the material. Then, they were mounted in resin for a better handling, after which they were metallographically prepared (ground up to 1200 SiC paper and polished with 6 and 1 µm diamond paste), followed by etching with Picral reagent (70 ml ethanol, 10 ml picric acid and 10 ml water). The average grain sizes in the base material and also in the upper zone of the affected layer were determined following the standard ASTME112 (standard test methods for determining average grain size). Besides, in order to determine the thickness of the affected layer of the treated specimens, five measurements were performed, and the average and standard deviation were obtained.

2.4 Roughness

Surface roughness measurements were performed on all specimens using a Diavite DH-6 roughness tester. Measurements were performed in eight random positions and directions over a length of 4.8 mm using a cut-off length of 0.8 mm following standard DIN4786.

2.5 Vickers microhardness profile

A Vickers microhardness profile was obtained on the cross section of all the SP treated specimens, in order to determine the depth and magnitude of the hardening due to the plastic deformation induced by each SP treatment. Measurements were performed by means of a microhardness tester Buehler Micromet 2100 applying a force of 25 gf during 15s (the load was applied gradually at a constant rate of 0.1 N/s).

The measurements were performed from the surface to the bulk of the material until hardness stabilization was attained, leaving a prudential distance between measurements to avoid abnormal results, as suggested by the standard ASTME92 (standard test methods for Vickers hardness and knoop hardness of metallic materials). The diagonals of the indentation marks were measured by optical microscope.

2.6 Residual stress and FWHM measurements

The residual stresses induced by different SP treatments performed on the AZ31B specimens were measured by means of X-ray diffraction using the unit X STRESSTECH 3000-G3R. The Cr-Kα radiation with a wavelength of 0.2291 nm was used, and the measurements were performed on the diffraction planes {1 0 4}, associated to a diffraction angle, 2θ, approximately equal to 152,4º. The $sen^2\psi$ method was employed, in which the residual stress is determined according to Equation 1:

$$\sigma_{\phi} = \left(\frac{E}{1+\nu}\right)_{(hkl)} \left(\frac{1}{d_{\phi 0 hkl}}\right)\left(\frac{\partial d_{\phi \psi hkl}}{\partial sin^2 \psi}\right) \qquad (1)$$

'E' and 'ν' are the elastic constants (elastic modulus and Poisson's coefficient) of the corresponding Mg alloy in the measured crystallographic plane, taken as 45 GPa and 0.35 respectively, 'd' is the interplanar spacing of the selected diffraction plane {hkl}, 'ψ' the tilt (rotation) angle and 'φ' the angle in the plane of the specimen. Diffraction peak detection was performed in 9 positions of the tilt angle, ψ, uniformly distributed between -45º and 45º, with an exposure time of 30 seconds in each position. The measurement was performed in three direction of the φ angle, -45º, 0º and 45º and the average value was obtained. All the parameters employed in the residual stress measurements are shown in Table 4.

Table 4. Parameters used in the residual stress measurements.

Measurement mode	χ modified	Radiation filter K_β	Vanadium
Maximum Voltage (kV)	30	Maximum Intesity (mA)	6.7
Exposure time (s)	50	Colimator diameter (mm)	1
Tilt angle ψ (º)	9 points between -45/+45	Goniometer rotation (Measurement direction) φ (º)	-45, 0, 45
Noise reduction	Parabolic	Peak fit method	Pseudo-Voigt

In order to define the in-depth residual stress profiles, thin layers of material were progressively removed by electropolishing in a Buehler PoliMat machine using a solution of 94% acetic acid and 6% perchloric acid under a voltage of 3 V. The width of the removed layer after each electropolishing stage was measured using a Mitutoyo micrometer, and this procedure was repeated until the residual stress became inexistent.

Additionally, the FWHM parameter (full width at half maximum) of the diffraction peaks was simultaneously measured. This parameter is related to grain distortion, dislocation density, and residual microstrains. FWHM can be considered as a work hardening index [42].

2.7 Corrosion tests

The corrosion behaviour of AZ31 specimens under different SP treatments was evaluated by means of potentiodynamic polarization tests carried out in Ringer's aqueous solution (concentration in g/l: 8.6 NaCl, 0.3 KCl and 0.33 $CaCl_2$, with pH≈7), simulating the chloride concentration in the human body environment. The tests were conducted at room temperature using a typical three-electrode cell with an Ag/AgCl electrode as a reference electrode, Pt as a counter-electrode and the specimen as working electrode.

After the Shot-Peening treatments, shot-peened samples were ultrasonic cleaned in ethanol in order to remove contaminants from the Shot Peening process and rests of the ceramic medium. Immediately, the specimens were directly submitted to potentiodynamic polarization tests after the SP treatments (without modifying their surface topography after the treatments). In a second batch, some of the SP treated specimens (500% at RT and 360ºC) were electropolished for some seconds (depending on the specimen surface topography) just to remove the highest peaks on the surface and attain a similar surface roughness to the one previously determined in the not-peened specimen (No-SP). Therefore, it would be possible to evaluate the influence of grain size, without the surface roughness interference, on the corrosion behavior of the SP treated specimens. Electropolishing process was conducted (in 94% acetic acid and 6% perchloric acid solution) without modifying any other surface property.

The potentyodinamic polarizations were performed from -100 to +200 mV vs. Ag/AgCl with respect to the open circuit potential (OCP) at a scan rate of 1 mV/s. A circular area of approximately 1 cm^2 was exposed to the electrolyte solution. The measurements were repeated two times per specimen using an Ivium PocketSTAT potentiostat.

The corrosion rate, CR, (in mm/year) was calculated using Faraday's law according to ASTMG102 (Standard practice for calculation of corrosion rates and related information from electrochemical measurements) as indicated in Equation 2:

$$CR\ [mm/year] = 3.27 \cdot 10^{-3} \cdot \frac{I_{corr} \cdot EW}{\rho} \qquad (2)$$

Where: 'I_{cor}' is the corrosion current density (μA/cm^2), 'ρ' is the density of the metal (g/cm^3) and 'EW' is the alloy equivalent weight.

3 Results

3.1 Microstructural characterization

Microstructure of the base material, as-received, and annealed at 400 ºC for 10 h, is shown in Figure 2. A complete microstructural homogenization is attained after the annealing stage. The effects of the previous cold rolling and forming process have been practically removed due to the annealing. The optical micrographs present an equiaxed grain microstructure, with an average grain size of 53±7 µm.

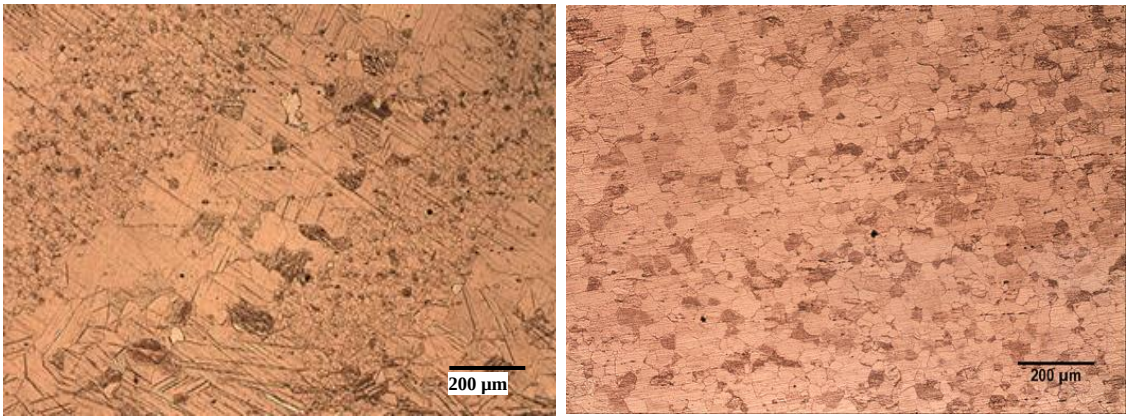

(a) *(b)*

Figure 2. Microstructure of AZ31 alloy: a) as received (100x), b) after annealing at 400 °C for 10 h (100x)

The microstructure of the top surface layer of the SP treated specimens are shown in
along with the measurements of the thickness of the affected depth. Average values are presented in Table 5.

In order to better observe the grain refinement extent in the affected zones, a detailed view is shown in Figure 4 and the average measurements of the grain sizes are collected in Table 6.

Having a look to the micrographs, it is possible to observe that the conventional SP treatments (100% coverage) performed at RT resulted in top layer with a considerably refined grain (GS less than 4 µm) up to a depth of around 60 µm. However, when increasing the surface coverage and applying SSP treatments (500 and 1000% coverage), the thickness of the affected depth approximately doubles (around 120 µm). Within this depth, a notable grain refinement was attained, forming a thick layer of ultrafine grains. Nevertheless, the changes induced under 500 and 1000% coverage levels were rather similar, which reveal the deformation threshold of the material at RT.

After the conventional SP treatment performed at 240ºC, the affected depth increased by around 40% compared to the same coverage at RT. Grain refinement was also attained although grain dimension was slightly bigger compared to the same treatment applied at RT (9 µm vs. 4 µm). On the other hand, the SSP treatments at 240ºC also induced a remarkable grain refinement (grains around 10-11µm); however, the grain dimension of these specimens was larger than those obtained at RT for the same coverage levels (10-11 vs. ultrafine grains). The thicknesses of the affected layers were measured to be quite similar to those obtained by the same treatments at RT (around 120 µm depth). In these cases, it is postulated that the higher amount of energy transmitted to the material (because of higher temperature) could have influenced the recrystallization process.

For the sample subjected to conventional SP treatments performed at 360ºC, the thickness of the affected zone was also two times higher than the same treatment at RT, and grain refinement was observed; however, also in this case, the grain size (13 µm) was slightly higher than lower temperature treatments (4 µm for RT and 9 µm for 240ºC). Nevertheless, the thickness of the affected layer for the SSP treated specimens at 360ºC was much higher compared to the previous series at RT and 240ºC (around 400 µm vs. 120 µm for RT and 120 µm for 240ºC). It is also to be noted that the specimens subjected to SSP at 360ºC, exhibited a significant increase in the grain

dimension (77-85 μm), even bigger than coarse grain. The cause may be the excess of thermal and mechanical energy, which lead to a notable recrystallization.

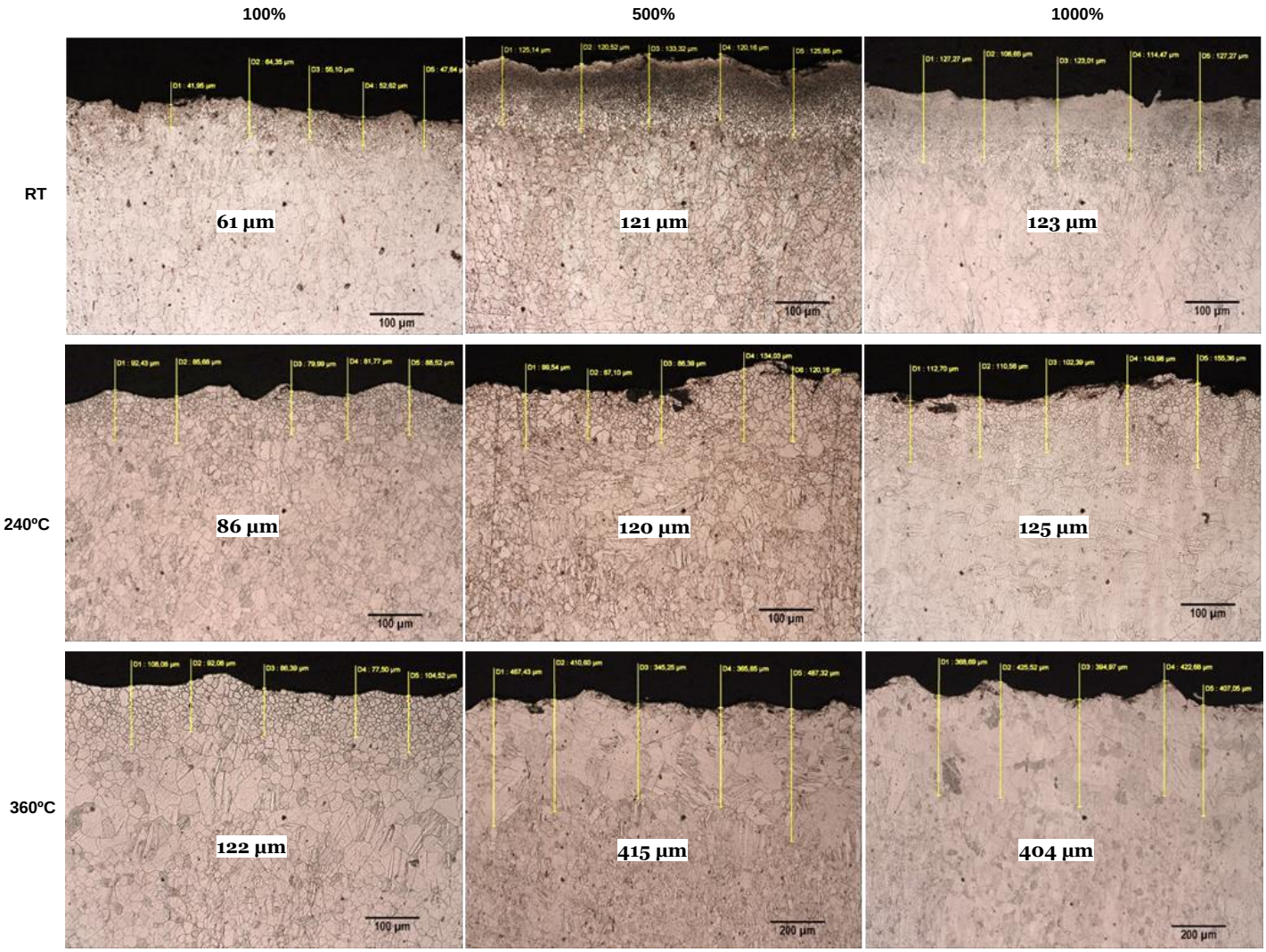

Figure 3. Microstructure of the top surface layer of AZ31 Mg alloy after different SP treatments. Thickness of affected layer (200x); 360ºC-500% and 360ºC1000%: 100x)

Table 5. Thickness of the affected layer after different SP treatments, measured from the optical micrographs in

		Coverage		
		100%	500%	1000%
Affected layer thickness [μm]	RT	61±5	121±6	123±10
	240ºC	86±5	120±13	125±21
	360ºC	122±6	415±62	404±23

COVERAGE

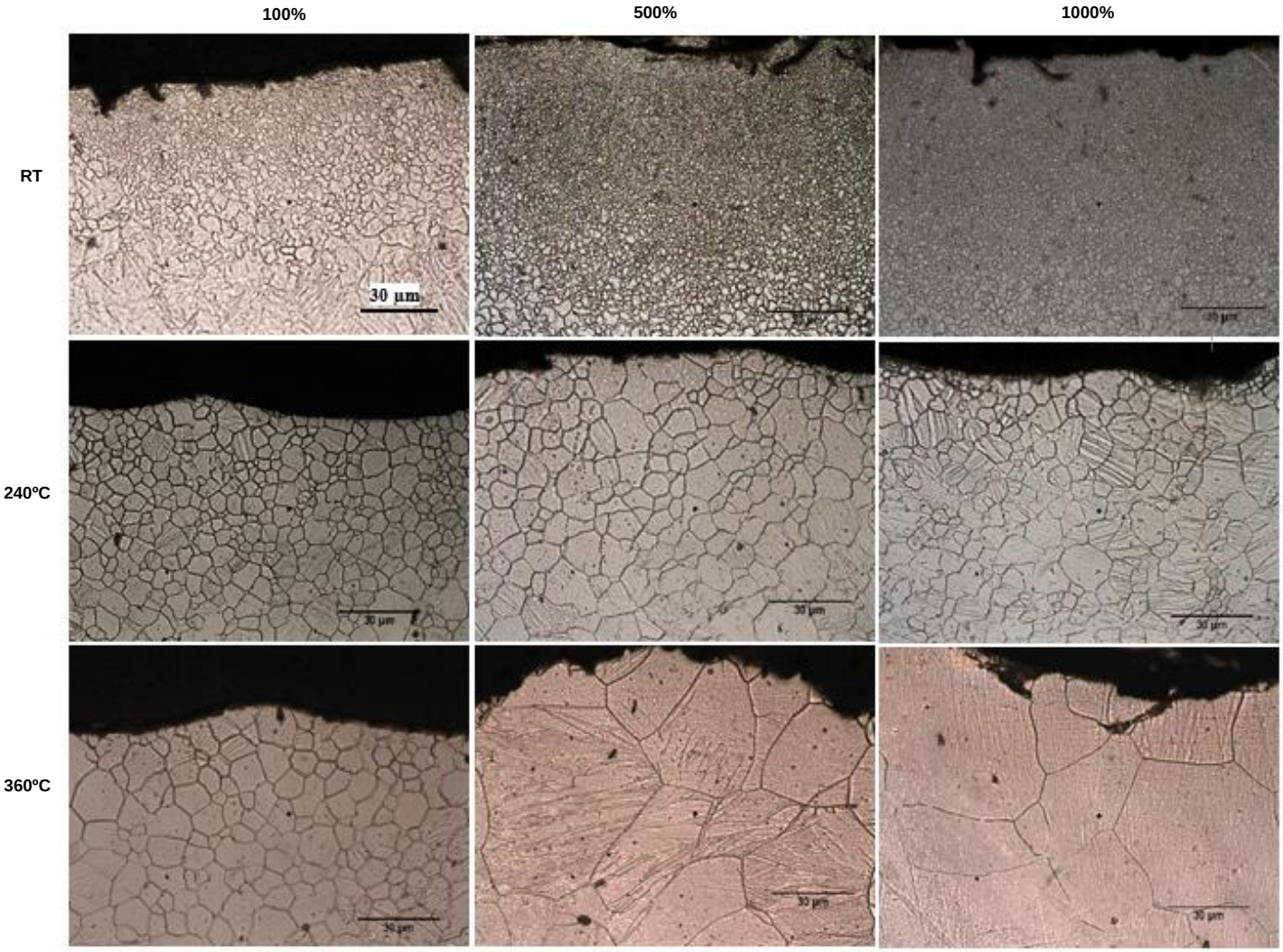

Figure 4. Microstructure of the top surface layer of AZ31 Mg alloy after different SP treatments (1000x)

Table 6. Average grain size (in µm) of the top surface layer of all the series, measured from the optical micrographs in Figure 4

Grain Size [µm]		Coverage		
		100%	500%	1000%
Temperature	RT	3.6±0.2	Ultrafine	Ultrafine
	240ºC	9.2±1.0	10.2±2.0	11.8±1.4
	360ºC	13.2±1.7	77.5±10.8	85.4±12.1

According to the presented results, it is possible to observe that plastic deformation induced notable grain refinement on the AZ31 specimens. Grain refinement was more remarkable under severe treatments at RT. Severe parameters also led to the highest thickness of the affected layer, although the effects were not proportional to the amount of kinetic energy. Grain refinement and thickness of the affected layer seem to reach a limit value, as also reported in [40] for the same alloy.

Conventional SP treatment at higher temperatures led to an increase in the thickness of the affected layer compared to RT treatments; the specimens treated at higher temperatures also induced grain refinement, although the grain dimensions were slightly higher than those obtained at RT. The thickness of the affected zone and grain dimension increased with temperature.

On the other hand, SSP at higher temperatures implies an excess of mechanical and thermal energy (these treatments are longer than conventional ones, and for this reason, specimens are under temperature effects for longer time); therefore, a different trend is observed regarding grain recrystallization in these specimens depending on the applied temperature. At 240 ºC, near magnesium recrystallization temperature, the thickness of the affected zone is quite similar to the one obtained at RT. Nevertheless, grain dimension is quite larger (~10 µm vs. ultrafine grains for RT series treated at the same coverage). On the other hand, at 360 ºC, above the magnesium recrystallization temperature, the same SSP treatment induces a recrystallization with larger grains, around 77-85 µm, higher than the grain dimension observed in the material core. The thickness of the affected layer in these specimens exceeded 400 µm.

3.2 Roughness

The arithmetic mean roughness parameter (R_a) obtained after the conventional and severe SP treatments are presented in Table 7 and Figure 5. R_a values increased with coverage level, and also with temperature treatment for the same amount of mechanical energy (same coverage level). This effect is attributed to the promoted ductility at higher temperatures.

In addition, some series, those with smaller and larger grain sizes (500% coverage at RT and at 360ºC respectively), were electropolished (EP) in order to reduce surface roughness caused by the SP process to attain surface roughness values close to that of the not-peened (No SP) specimens (R_a~2µm). Accordingly, the effect of grain size on corrosion behaviour, avoiding surface roughness contribution, could be evaluated as discussed later. After electropolishing, R_a values decreased from 8.8 to 3 µm the 500% sample treated at RT and from 12.1 to 3 µm in the 500% sample treated at 360ºC.

Table 7. Roughness (R_a) evolution depending on the surface treatment

Surface treatment	Temperature (°C)	Roughness parameter R_a (µm)
No SP	---	2.0 ± 0.14
100% coverage	RT	7.9 ± 0.82
	240	10.1 ± 0.88
	360	12 ± 0.71
500% coverage	RT	8.8 ± 0.14
		3.0 (after EP) ± 0.12
	240	11.1 ± 0.61
	360	12.1 ± 0.14
		3.0 (after EP) ± 0.10

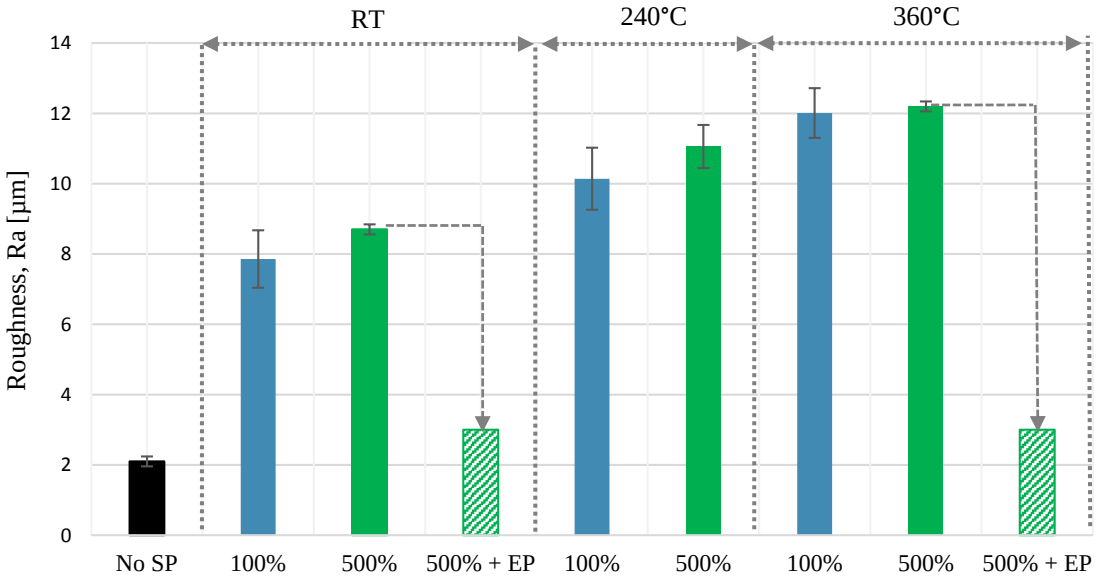

Figure 5. R_a roughness evolution under the different applied SP surface treatment

3.3 Microhardness profile

Vickers microhardness profiles obtained from the surface to the bulk of all the shot-peened specimens are shown in

Figure 6. Additionally, Table 8 gathers the values of the hardness peak and the hardened depth. The hardness of the annealed samples is 60 HV (the same as the shot peened sample's core material).

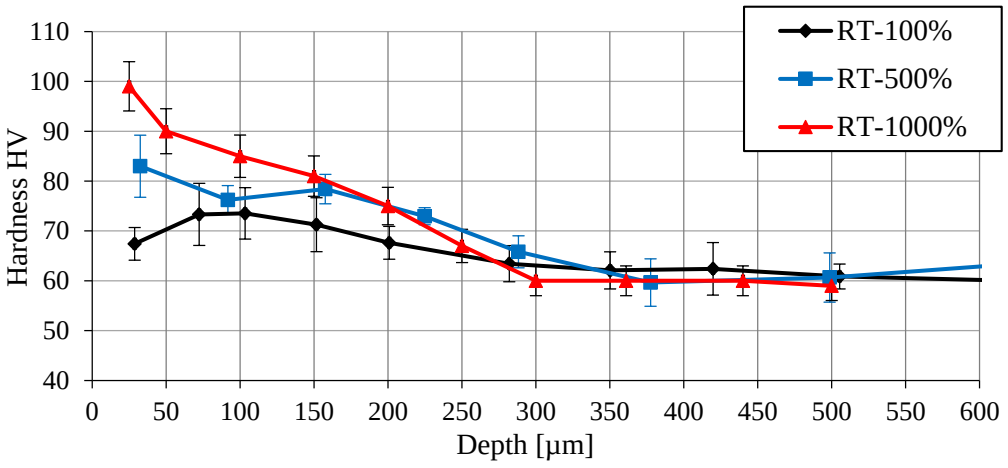

(a)

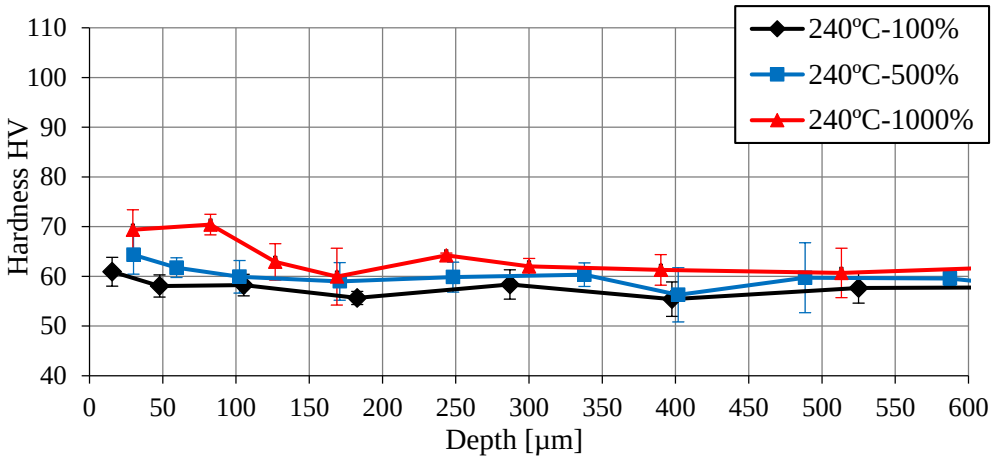

(b)

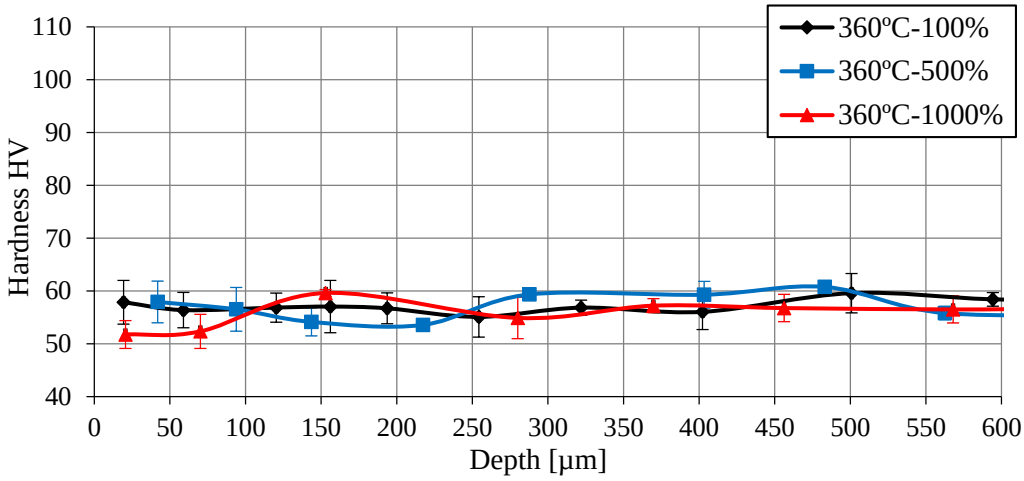

(c)

Figure 6. Vickers microhardness profile of the SP specimens at (a) RT, (b) 240°C and (c) 360°C

According to the obtained results, it is possible to observe a considerable increment of hardness in the upper layer of the specimens treated at RT. This effect was more notable under the highest coverage levels. The surface hardness increments were quantified as 23%, 38% and 65% for 100%, 500% and 1000% coverage, respectively. The thickness of the affected zone at RT seemed to be practically (constant around 300 µm) and not affected by the coverage level.

However, in the case of warm treatments, an equilibrium between work hardening induced by kinetic energy and the softening due to the high temperature seemed to take over. In fact, at 240 ºC, only in the case of a maximum coverage level (1000%) a slight increment of hardness is noticed, until a depth of 150 µm. At 360 °C, independently of the applied coverage level, the hardening effects were null, even noticing a slight softening in the topmost layer of 150 µm thick.

Table 8. HV values at the surface and hardened depth for all the series obtained from the microhardness profiles

Treatment Temperature	Coverage	HV_{peak}	Depth of the hardened layer [µm]
RT	100%	74±5.2	350
	500%	83±6.2	350
	1000%	99±4.7	300
240 ºC	100%	61±2.9	50
	500%	64±3.9	100
	1000%	70±4.0	150
360 ºC	100%	58±4.1	---
	500%	58±3.9	---
	1000%	60±2.6	---

3.4 Residual stress profile

The obtained in-depth residual stress profiles, shown in Figure 7, represent the average stress (measured in three directions of -45, 0 and 45º) along the affected layer of the AZ31 after different SP treatments. The residual stress levels induced in the specimens was very small after conventional and severe SP treatments at RT (<70 MPa in all cases), if compared with different materials submitted to similar treatments [28-35]. These values were further decreased after warm SP. However, the thickness of the affected layer increased after SSP treatments.

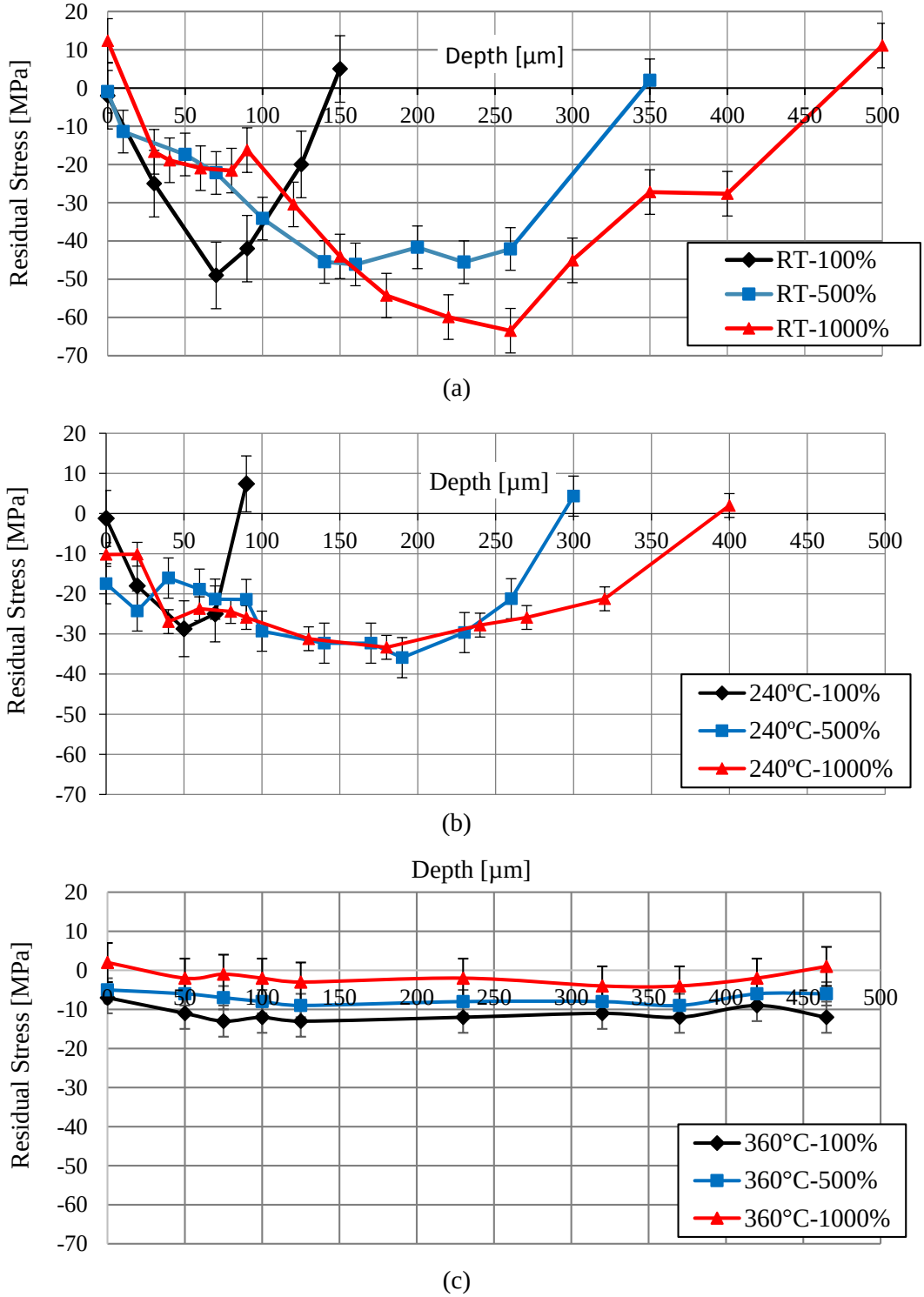

Figure 7. Residual stress profile of the SP specimens at (a) RT, (b) 240 °C and (c) 360 °C

3.5 FWHM profile

FWHM profiles (Figure 8), serve as an index for hardening [42], and are in accordance with the microhardness trends shown in

Figure 6. Thus, again the specimens treated at RT exhibit a considerable hardening (Figure 8(a)) at all coverage levels; while specimens treated under higher temperatures did not experience any noticeable change, regardless the applied coverage.

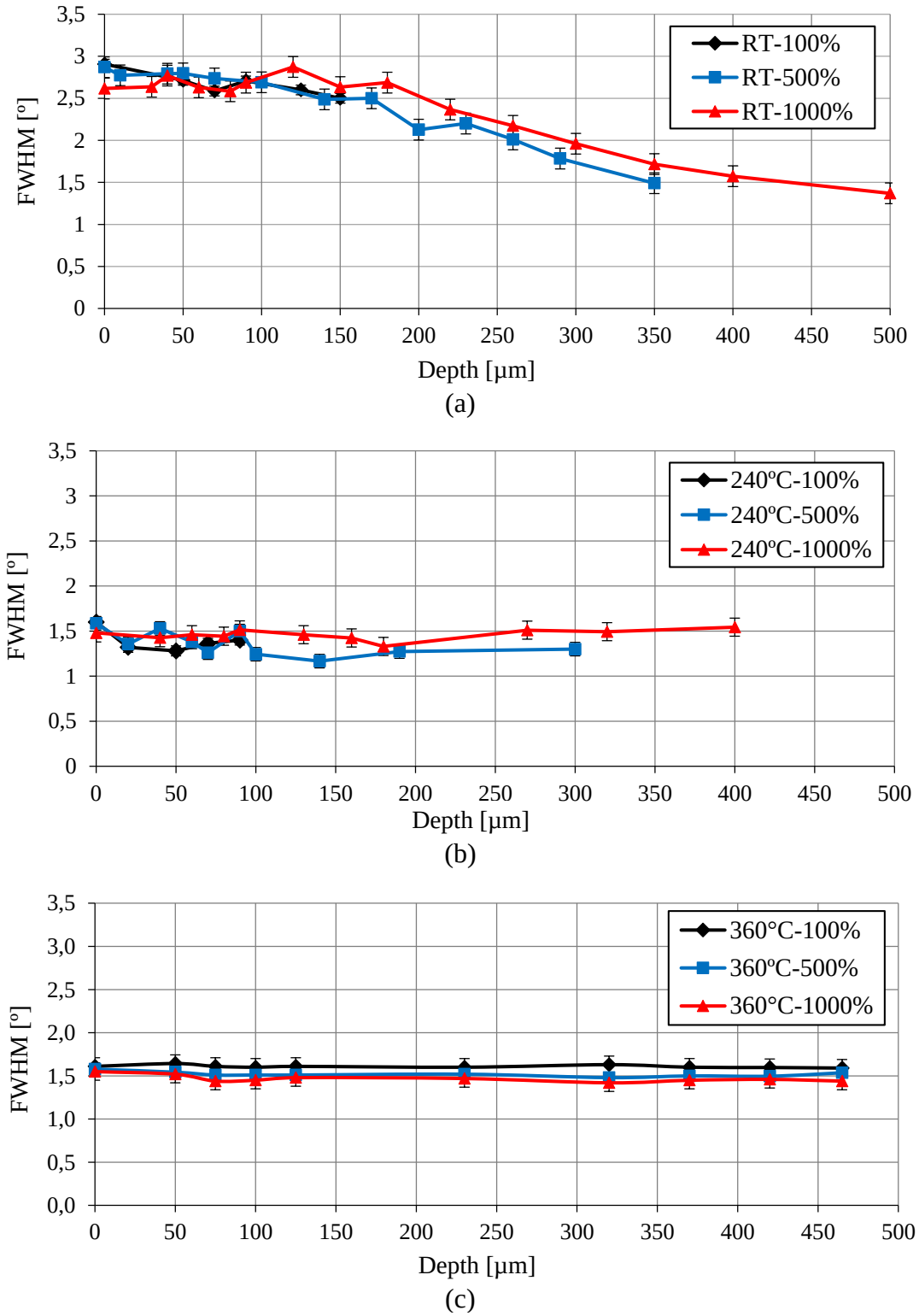

Figure 8. FWHM profile of the SP specimens at (a) RT, (b) 240°C and (c) 360°C

3.6 Corrosion tests

Figure 9 compares the potentiodynamic polarization curves of the AZ31 specimens under different treatments: not-peened (No SP) and SP treatments at different temperatures (RT, 240 ºC and 360 ºC) under different coverage levels (100% in Figure 9(a) and 500% in Figure 9(b)). The specimens treated under the highest coverage (1000%) were not considered for corrosion tests as the induced microstructural changes in these specimens were similar to those achieved in specimens treated with 500% coverage. The obtained corrosion parameters are listed in Table 9, where 'I_{cor}' is the corrosion intensity, 'E_{cor}' is the corrosion potential, 'CR' is the corrosion rate and 'β_a' and 'β_c' are the slopes of the anodic and cathodic polarization curves, respectively.

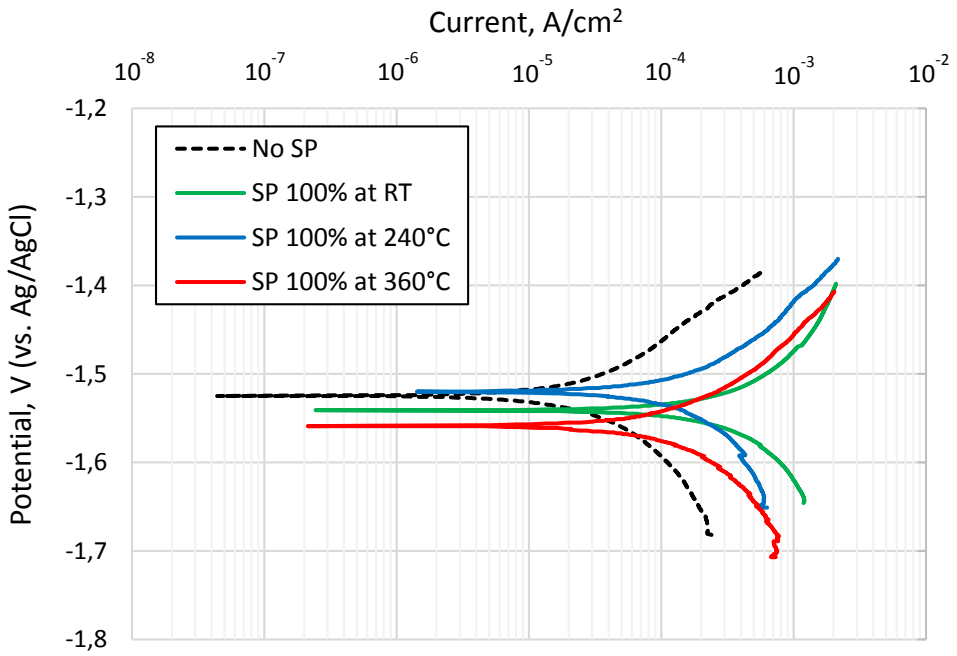

(a)

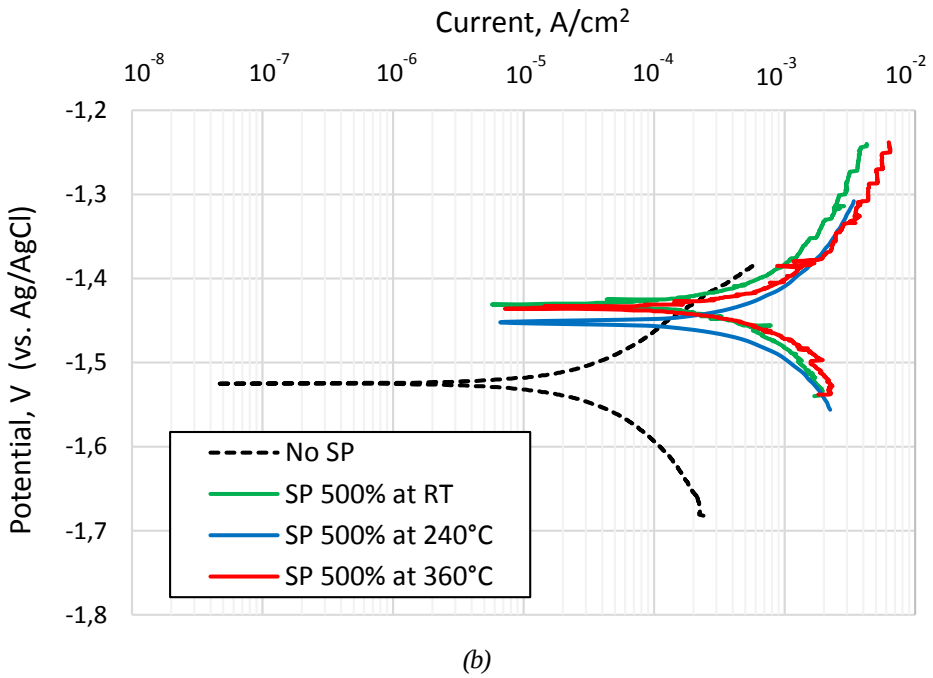

(b)

Figure 9. Potentiodynamic polarization curves of AZ31 specimens in Ringer's solution.

(a) Coverage level of 100% at RT, 240 ºC and 360 °C and (b) Coverage level of 500% at RT, 240 ºC and 360°C

Table 9. Electrochemical corrosion parameters obtained by Tafel extrapolation analysis of the measured Potentyodinamic curves on AZ31 specimens under different SP treatments

Coverage	Temperature	Corrosion parameters				
		I_{cor} [µA/cm^2]	E_{cor} [mV]	CR [mm/year]	β_a [mV]	β_c [mV]
No SP		29	-1509	0.66	65	155
100%	RT	120	-1538	2.74	40	90
	240°C	126	-1506	2.87	60	168
	360°C	141	-1538	3.22	59	158
500%	RT	251	-1424	5.72	45	110
	240°C	316	-1438	7.20	46	112
	360°C	355	-1423	8.10	42	100

As a summary, corrosion results obtained for surface coverages of 100% and 500% under RT, 240ºC and 360ºC, are presented in Figure 10 after the aforementioned SP treatments.

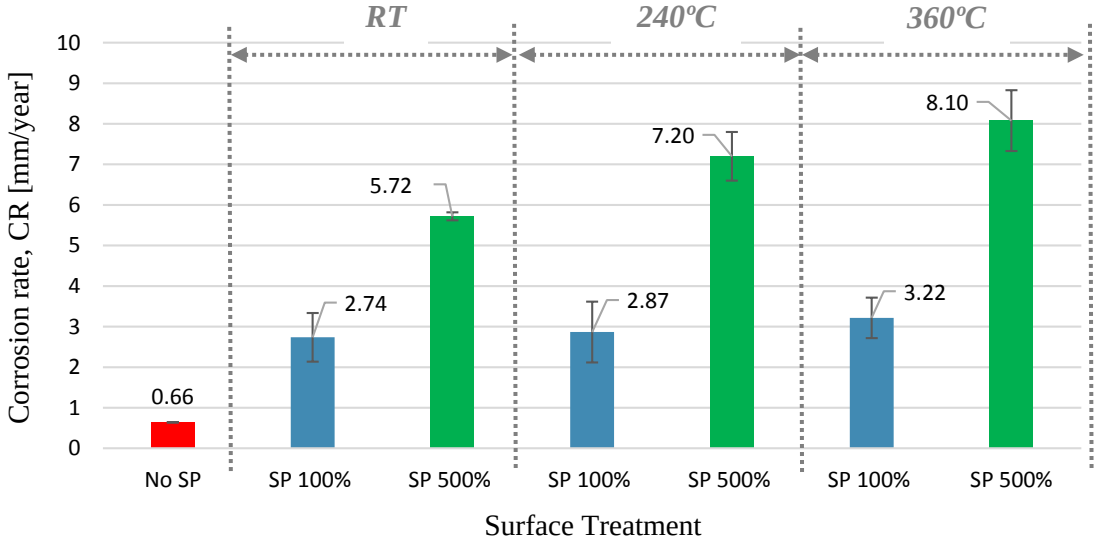

Figure 10. Corrosion rate (in mm/year) obtained under the different surface treatments on the AZ31 specimens

The results indicate that corrosion rate (CR) of all SP treated specimens (both at 100 and 500% coverage), is much higher that the not-peened specimen, regardless the treatment temperature (see Figure 10). This fact might be explained due to the highest surface roughness values (see Figure 5) induced by the SP treatments, as will be further discussed. In addition, the comparison of the SP treatments indicates that under a coverage level of 100%, the corrosion rate remained practically constant (between 2.7 and 3.2 mm/year) for all the employed treatment temperatures. However, with the application of a coverage level of 500%, the corrosion rates were much higher, and increased considerably with the treatment temperature, as can be seen in Figure 10.

4 Discussion

To evaluate the SP effect on the corrosion properties of the AZ31 specimens, surface properties such as: surface roughness, grain size and residual stresses must be taken into consideration. Firstly, surface roughness (R_a) generated after SP treatment on the surface layer due to the severe plastic deformation is known to play an important role on the corrosion behavior, as also confirmed in Figure 11. These data reveal that regardless the coverage (100 or 500%) and the treatment temperature (RT, 240 ºC or 360 ºC), R_a parameters of all SP treated series were always higher than 7 µm. This high surface roughness is known to contribute to the increase the corrosion

rates (CR) for these series with respect to the not-peened ones (R_a~2µm). The results confirm that the smoothest surface finish induced lower corrosion rate thanks to the lower number of active sites for preferential local corrosion [43, 44].

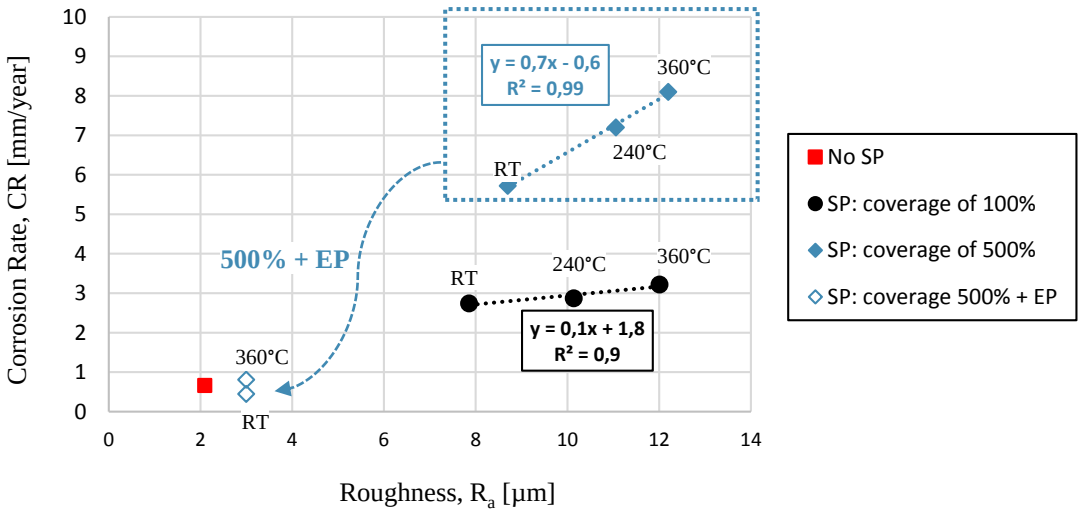

Figure 11. Effect of roughness (R_a) on corrosion resistance of AZ31 Mg alloy

Secondly, to study the effect of grain size caused by the SP treatment on the corrosion resistance, the surface roughness effect was separated, without altering the internal layer properties of the AZ31 specimens, by means of a slight electropolishing process. Hence, series with notable differences in grain dimension were selected to evaluate the influence of grain size on corrosion behavior; i.e., RT at 500% coverage and 360 ºC at 500% coverage, which have ultrafine and 70 µm grains close to the surface, respectively. After the electropolishing process, surface roughness (R_a) of the specimens decreased from 8.8 to 3 µm for RT at 500% coverage series and from 12.1 to 3 µm for 360 ºC and 500% coverage specimens (see Figure 11), being quite similar to the surface roughness determined in the not-peened series (2 µm). Therefore, the corrosion behavior of these specimens could be directly compared to find the contribution of their distinctive grain size, eliminating the effect of the surface roughness, as they exhibited quite similar R_a values. Potentiodynamic polarization curves before and after the electropolishing process for series RT at 500% coverage and 360 ºC at 500% coverage series are shown in Figure 12. The obtained data from these curves are represented in Table 10 and Figure 13.

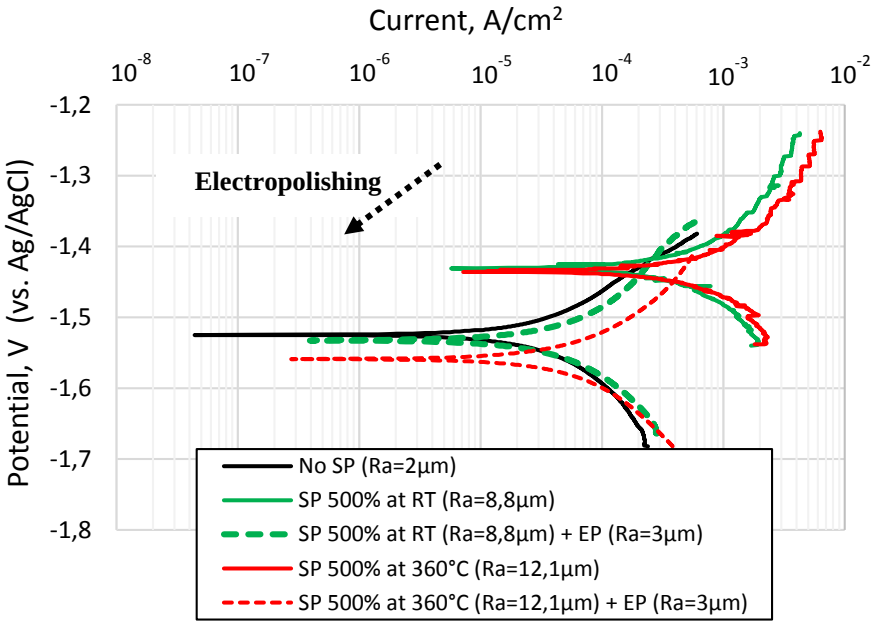

Figure 12. Potentiodynamic polarization curves of AZ31 specimens in Ringer's solution before and after electropolishing (EP)

Table 10. Electrochemical corrosion parameters obtained by Tafel extrapolation analysis of the measured Potentyodinamic curves on AZ31 specimens under 500% coverage before and after electropolishing (EP) compared to the not-peened (No SP) specimen

Coverage	Temperature	Roughness, R_a [µm]	Corrosion parameters				
			I_{cor} [µA/cm^2]	E_{cor} [mV]	CR [mm/year]	β_a [mV]	β_c [mV]
No SP		2.0µm	29	-1509	0.66	65	155
500%	RT	After SP → R_a=8.8µm	251	-1424	5.72	45	110
		SP + EP → R_a=3µm	20	-1525	0.45	31	92
	360°C	After SP → R_a=12.1µm	355	-1423	8.10	42	100
		SP + EP → R_a=3µm	36	-1500	0.82	46	98

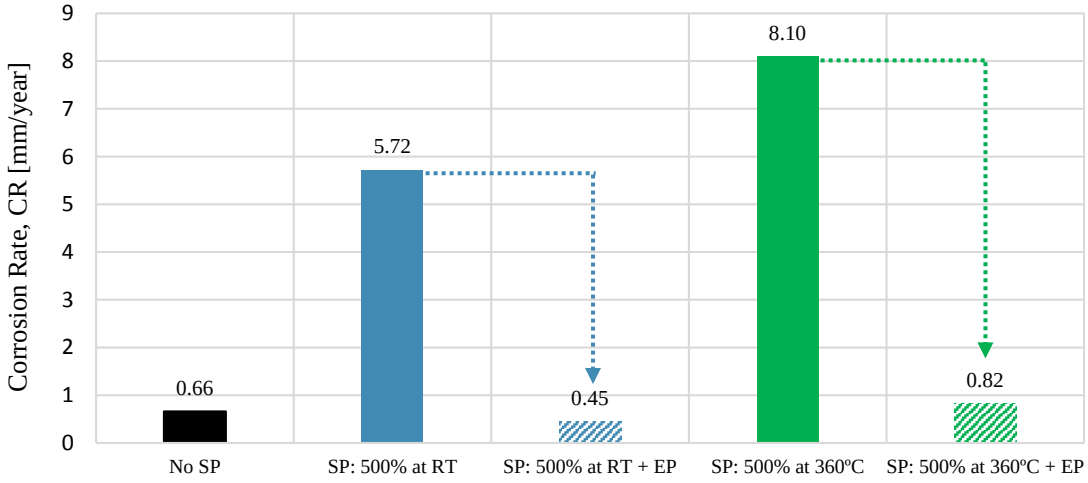

Figure 13. Corrosion rates in Ringer's solution before and after electropolishing (EP)

Table 11 summarizes R_a parameters, grain dimension and CR of the not-peened specimen, RT-500% +EP and 360 ºC-500% +EP series, respectively.

Table 11. Comparing the characteristics of the specimens after the electropolishing process

Treatment	Ra [µm]	GS [µm]	CR [mm/year]
No SP	2.0	53	0.66
SP: 500% at RT + EP	~3.0	UF	0.45
SP: 500% at 360ºC + EP	~3.0	77.5	0.82

According to these results, the corrosion behavior of the series with a coverage of 500%, shot peened both at RT and 360ºC, improved notably after the applied electropolishing step; the corrosion rates of these series decreased from 5.72 to 0.45 mm/year and from 8.10 to 0.82 mm/year, respectively (Figure 13). These results highlight the crucial role of surface roughness on the corrosion behavior of AZ31 specimens.

Regarding the effect of grain dimension, RT-500%+EP specimen with ultrafine grains showed the best corrosion resistance (0.45 mm/year), while corrosion rate of the 360ºC-500 %+EP specimen with an average grain size around 77.5µm was slightly higher, i.e., 0.82 mm/year (see Table 11).

Besides, it is also important to mention that the series with ultrafine grains (RT-500%+EP) showed a corrosion rate of 0.45 mm/year, even lower that the not-peened specimens which exhibited a corrosion rate of 0.66 mm/year and GS of 53µm. The influence of grain dimension on CR can be explained by considering the increased grain boundaries density as a consequence of grain size reduction; the higher number of grain boundaries have been reported to act as corrosion barrier efficient in inhibiting the corrosion [45, 46], as demonstrated in decreased corrosion rates (CR) presented in Table 11.

On the other hand, the corrosion resistance of the 360 ºC-500 %+EP specimens was not improved with respect to the not-peened (No SP) series, presumebly due to its higher grain size (77.5 µm) and consequently, the lower grain boundaries density (less barriers to inhibit corrosion).

These data analisys have been also represented in Figure 14. The results show the important influence of grain dimension on corrosion behavior for specimens with similar surface roughness. Consequently, it is observed that grain refinement and the resultant ultrafine grains can contribute to improving corrosion resistance.

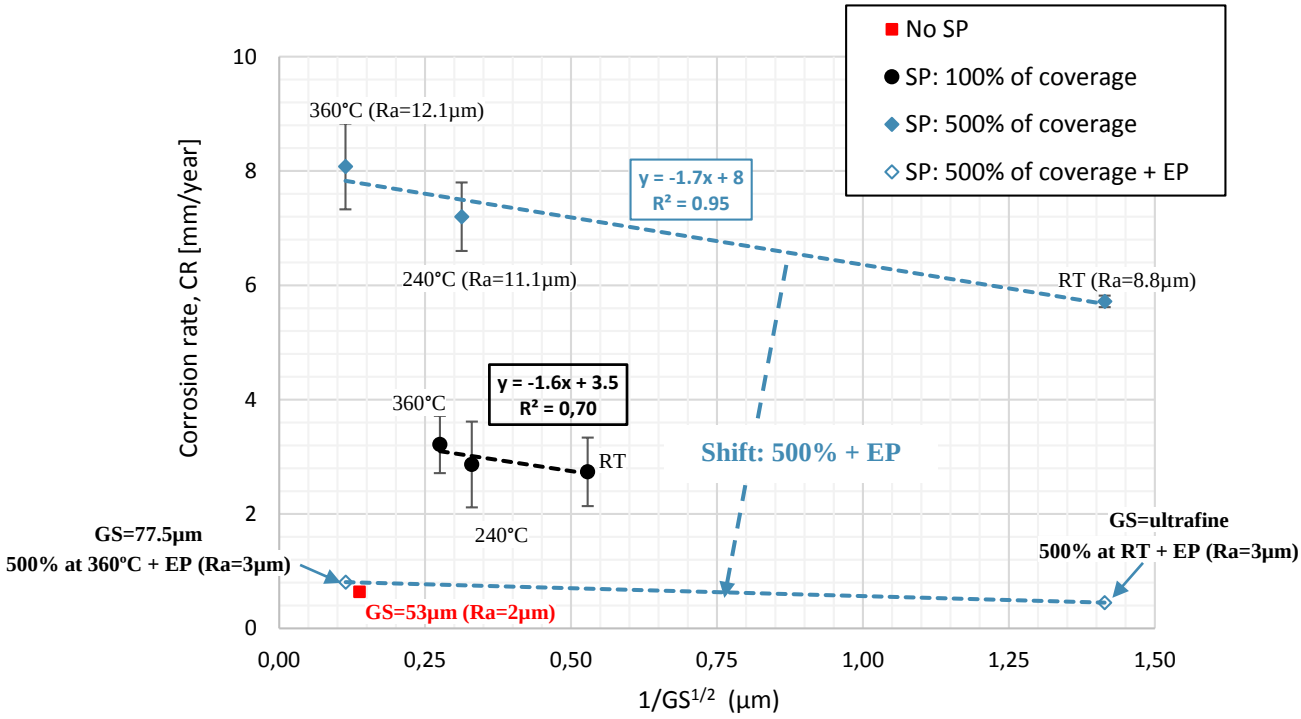

Figure 14. Effect of grain size on corrosion resistance of AZ31 Mg alloy

Another important parameter, which could also influence the corrosion behavior of the specimens, is the residual stresses field induced by the SP treatments. Some authors [22, 37] have revealed that residual stresses induced by SP might play a key role on corrosion behavior, contributing to an increased in corrosion rate. According to the presented results, the residual stresses induced in the surface layer of AZ31 specimens were barely significant, being very close to zero MPa (Figure 7), also in agreement with previous studies [35]. Therefore, it is assumed that their contribution to corrosion behavior could be neglected in this work.

According to the obtained results, the SP treatments might be an effective method to improve the corrosion resistance of AZ31 Mg alloy; however, the process parameters and the resultant surface topography play a significant role on determining the corrosion resistance of the treated specimens.

5 Conclusions

On the basis of the obtained results, the following conclusions can be drawn:

- Shot peening and severe shot peening treatments, performed at room temperature, 240 ºC and 360 ºC modified the microstructure of the top surface layer of the AZ31 specimens. Severe shot peening at room temperature induced significant refinement of the grains size in the upper surface layer; whereas at temperature 240ºC a less notable refinement occurred. The thickness of the affected layer was similar for the treatments performed at room temperature and at 240ºC. Nevertheless, severe shot peening performed at 360ºC induced a remarkable grain growth.

- Microhardness and FWHM measurements showed a notable work hardening effect (hardened depth around 300-400 µm) in the shot peened specimens treated at room temperature, which increased with the applied coverage. When increasing the treatment temperature, the hardening effect dropped and vanished at 360 ºC. A possible cause may be the equilibrium between the work hardening effect generated by the high energy impacts and the softening induced by high temperature.

- Investigating the corrosion behaviour of fine-grained AZ31 magnesium alloy in Ringer Lactato solution indicated that, in the initial conditions, the corrosion rate of the shot peened specimens (100 and 500% coverage) was much higher compared to the not-peened material. This effect is explained due to the high surface roughness caused by the multiple high energy impacts during shot peening. The series with higher surface roughness showed higher corrosion rates.

- Under similar surface roughness conditions, the influence of grain dimension on corrosion behavior was found to be notable. In particular, corrosion rate decreased for the series of the same surface roughness but with smaller grain size. The best results were obtained for the treatment performed with 500% coverage at room temperature followed by an electropolishing step applied to decrease the surface roughness.

On the base of the previous points, it can be concluded that grain refinement caused by the severe plastic deformation induced by shot peening treatments shows the potential to improve the corrosion behaviour of AZ31 Mg alloy. Further investigations are needed to orient the choice of the optimal treatment parameters and to define the most appropriate post-processing in view of obtaining the desired surface finishing

Acknowledgments

Authors also thank the financial support received from the Principado de Asturias government through the FC-GRUPIN-IDI/2018/000134 project.

References

[1] B.B. Clow, Advanced Materials & Processes 10 (1996) 33.
[2] L.W.F. Mackenzie, M. Pekguleryuz. The influences of alloying additions and processing parameters on the rolling microstructures and textures of magnesium alloys. Materials Science and Engineering A 480 (2008) 189-197.
[3] Usman Riaz, Ishraq Shabib, Waseem Haider. The current trends of Mg alloys in biomedical applications: a review. Journal of Biomedical Materials Research Part B: Applied Biomaterials 107 (2019) 1970-1996.

[4] Kathryn F. Farraro, Kwang E. Kim, Savio L-Y. Woo, Jonquil R. Flowers, Matthew B. McCullough. Revolutionizing orthopaedic biomaterials: The potential of biodegradable and bioresorbable magnesium-based materials. Journal of Biomechanics 47 (2014) 1979-86.
[5] Chen Liu, Zheng Ren, Yongdong Xu, Song Pang, Xinbing Zhao, Ying Zhao. Biodegradable Magnesium Alloys Developed as Bone Repair Materials: A Review. 2018 (2018) 1-15.
[6] Staiger M.P., Pietak, A.M., Huadmai J., Dias G. Magnesium and its alloys as orthopedic biomaterials: a review. Biomaterials 27(9) (2006) 1728-34.
[7] Jasmawati N., Fatihhi S.J., Putra A.M.S., Syahrom A., Haru, M.N., Öchsner A., Abdul Kadir M.R. Mg-based porous metals as cancellous bone analogous material: A review. Sage journals (2015) 544–556
[8] Wu, Y.F., Wang, Y.M.Jing, Y.B.Zhuang, J.P.,Yan, J.L.,Shao, K.Jin, M.S.,Wu, C.J.,Zhou,Y. In vivo study of microarc oxidation coated biodegradable magnesium plate to heal bone fracture defect of 3 mm width. Colloids and Surfaces B: Biointerfaces 158 (2017) 147-156.
[9] J.A. Cowan. The Biological Chemistry of Magnesium. VCH Publishers, Inc.: New York. (1995).
[10] Peng Tian and Xuanyong Liu. Surface modification of biodegradable magnesium and its alloys for biomedical applications. Regenerative Biomaterials 2(2) (2015) 135–151.
[11] T.S.N. Sankara Narayanan, Il-Song Park, Min-Ho Lee. Surface modification of magnesium and its alloys for biomedical applications, Volume 1: Biological Interactions, Mechanical Properties and Testing. Publisher: Woodhead Publishers (2015).
[12] Andrej Atrens, Guang-LingSong, FuyongCao ZhimingShi, K.Bowen. Advances in Mg corrosion and research suggestions. Journal of magnesium and alloys 1(3) (2013) 177-200.
[13] Hassel T., Bach F.-W., Krause C., Wilk P. Corrosion protection and repassivation after the deformation of magnesium alloys coated with a protective magnesium fluoride layer. Proceedings of the 2005 TMS Annual Meeting USA (2005) 485–490.
[14] Kuhlmann J., Bartsch I., Willbold E., Schuchardt S., Holz O., Hort N., Höche D., Heineman WR., Witte F. Fast escape of hydrogen from gas cavities around corroding magnesium implants. Acta Biomaterialia 9(10) (2013) 8714–8721.
[15] Wang H., Shi Z. In vitro biodegradation behavior of magnesium and magnesium alloy. Journal of Biomedical Materials Research Part B: Applied Biomaterials 98(2) (2011) 203–209.
[16] Gray J. E., Luan B. Protective Coatings on Magnesium and Its Alloys. A Critical Review. ChemInform 33(26) (2002).
[17] Turhan M. C., Lynch R., Killian M. S., Virtanen S. Effect of acidic etching and fluoride treatment on corrosion performance in Mg alloy AZ91D (MgAlZn). Electrochimica Acta 55(1) (2009) 250-257.
[18] M. Assadian, M. H. Idris, M. M. Taheri, M. Rezazadeh Shirdar and D.Almasi. Effects of Alkaline Treatment on Corrosion Behavior of Biodegradable Magnesium. Advanced Materials Research 1125 (2015) 441-444.
[19] Li L., Gao J., Wang Y. Evaluation of cyto-toxicity and corrosion behavior of alkali-heat-treated magnesium in simulated body fluid. Surface and Coatings Technology 185(1) (2004) 92–98.
[20] Z. Pu, G-L. Song, S. Yang, J.C. Outeiro, O.W. Dillon Jr., D.A. Puleo e, I.S. Jawahir. Grain refined and basal textured surface produced by burnishing for improved corrosion performance of AZ31B Mg alloy. Corrosion Science 57 (2012) 192–201
[21] P. Klimanek, A. Pötzsch. Microstructure evolution under compressive plastic deformation of magnesium at different temperatures and strain rates. Materials Science and Engineering A 324 (2002) 145–150.
[22] K. D. Ralston, N. Birbilis. Effect of Grain Size on Corrosion: a Review. CORROSION 66(7) (2010) 075005-075005-13.
[23] G. Ben Hamu, D. Eliezer, L. Wagner. The relation between severe plastic deformation microstructure and corrosion behavior of AZ31 magnesium alloy. Journal of Alloys and Compounds 468 (2009) 222–229.
[24] Yichi Liu, Debao Liu, Chen Yoy, Minfang Chen. Effects of grain size on the corrosion resistance of pure magnesium by cooling rate-controlled solidification. Frontiers of Materials Science 9 (2015) 247–253.

[25] H. Kovaci, Y.B. Bozkurt, A.F. Yetim, M.Aslan, A. Çelik. The effect of surface plastic deformation produced by shot peening on corrosion behavior of a low-alloy steel. Surface and Coatings Technology 360 (2019) 78-86.
[26] Shu-xu WU, Shou-ren WANG, Gao-qi WANG, Xiu-chun YU, Wen-tao LIU, Zheng-qi CHANG, Dao-sheng WEN. Microstructure, mechanical and corrosion properties of magnesium alloy bone plate treated by high-energy shot peening. Trans. Nonferrous Met. Soc. China 29 (2019) 1641-1652.
[27] V.Azar, B.Hashemi, Mahboobeh Rezaee Yazdi. The effect of shot peening on fatigue and corrosion behavior of 316 stainless steel in Ringer's solution. Surface and Coatings Technology 204 (2010) 3546-3551.
[28] AF Ciuffini, S Barella, LB Peral Martínez, C Mapelli, I Fernández Pariente. Influence of microstructure and shot peening treatment on corrosion resistance of AISI F55-UNS S32760 super duplex stainless steel. Materials 11(6) (2018) 1038.
[29] IF Pariente, M Guagliano. About the role of residual stresses and surface work hardening on fatigue ΔK_{th} of a nitrided and shot peened low-alloy steel. Surface and Coatings Technology 202 (13) (2008) 3072-3080.
[30] E. Real, C. Rodriguez, F. J. Belzunce, P. Sanjurjo, A. F. Canteli, I. F. Pariente. Fatigue behaviour of duplex stainless steel reinforcing bars subjected to shot peening. Fatigue and Fracture of Engineering Materials and Structures 32 (2009) 567–572.
[31] Inés Fernández Pariente, Mario Guagliano. Influence of Shot Peening Process on Contact Fatigue Behavior of Gears. Materials and Manufacturing Processes 24 (2009) 436–1441.
[32] J González, LB Peral, C Colombo, I Fernández-Pariente. A study on the microstructural evolution of a low alloy steel by different shot peening treatments. Metals 8(3) (2018) 187.
[33] Sara Bagherifard, Sebastian Slawik, Inés Fernández-Pariente, Christoph Pauly, Frank Mücklich, Mario Guagliano. Nanoscale surface modification of AISI 316L stainless steel by severe shot peening. Materials and Design 102 (2016) 68–77.
[34] Sara Bagherifard, Inés Fernandez-Pariente, Ramin Ghelichi, Mario Guagliano. Severe shot peening to obtain nanostructured surfaces: process and properties of the treated surfaces. Handbook of Mechanical Nanostructuring (2015) 299-323.
[35] S Bagherifard, DJ Hickey, S Fintová, F Pastorek, I Fernandez-Pariente, Michele Bandini, Thomas J. Webster, Mario Guagliano. Effects of nanofeatures induced by severe shot peening (SSP) on mechanical, corrosion and cytocompatibility properties of magnesium alloy AZ31. Acta Biomaterialia 66 (2018) 93–108.
[36] M. Hilpert, L. Wagner. Fatigue performance of a shot peened high-strength magnesium alloy. Transactions on Engineering Sciences 25 (1999) 331-340.
[37] Zhang P, Lindemann, J. Influence of shot peening on high cycle fatigue properties of the high-strength wrought magnesium alloy AZ80. Scripta Materialia 52(6) (2005) 485-490.
[38] S Bagherifard. Enhancing the Structural Performance of Lightweight Metals by Shot Peening. Advanced Engineering Materials (2019) 1-21
[39] Y. Huang, W. C. Liu and J. Dong. Surface characteristics and fatigue performance of warm shot peened wrought magnesium alloy Mg–9Gd–2Y. Materials Science and Technology 30(12) (2014).
[40] Y. Tang and J.A. El-Awady. Formation and slip of pyramidal dislocations in hexagonal close-packed magnesium single crystals. Acta Materialia 71 (2014) 319–332.
[41] Anna Dziubińska, Andrzej Gontarz, Karina Horzelska, Paweł Pieśko. The Microstructure and Mechanical Properties of AZ31 Magnesium Alloy Aircraft Brackets Produced by a New Forging technology. Procedia Manufacturing 2 (2015) 337 – 341.
[42] Noyan, I.C.; Cohen, J.B. Residual Stress Measurement by Diffraction and Interpretation; Springer: New York, NY, USA, (1987).
[43] E.B. Barmatov, Dmitry Eskin, Trevor Hughers. Effect of surface roughness on corrosion behaviour of low carbon steel in inhibited 4M hydrochloric acid under laminar and turbulent flow conditions. Corrosion Science 103 (2015).
[44] Sara Bagherifard, Mauro Filippo Molla, Daniel Kajanek, Riccardo Donnini, Branislav Hadzim, Mario Guagliano. Accelerated biodegradation and improved mechanical performance of pure iron through surface grain refinement. Acta Biomaterialia 98 (2019) 88-102.

[45] J. Liao, M. Hotta, A. Koshi. Effect of oxygen content on impact toughness of a fine-grained magnesium alloy. Material Letters 65(19-20) (2011) 2995–2999.
[46] N. Aung, W. Zhou. Effect of grain size and twins on corrosion behaviour of AZ31B magnesium alloy. Corrosion Science 52 (2010) 589–594.